Unraveling the Spin Polarization of the $\nu = 5/2$ Fractional Quantum Hall State

L. Tiemann, *et al.*

Science **335**, 828 (2012);
DOI: 10.1126/science.1216697

7. J. Harrow *et al.*, *Genome Biol.* **7** (suppl. 1), S4, 1 (2006).
8. http://vat.gersteinlab.org/
9. See supporting material on *Science* Online.
10. R. E. Mills *et al.*; 1000 Genomes Project, *Nature* **470**, 59 (2011).
11. A. Uzumcu *et al.*, *J. Med. Genet.* **43**, e5 (2006).
12. D. G. MacArthur *et al.*, *Nat. Genet.* **39**, 1261 (2007).
13. Y. Xue *et al.*, *Am. J. Hum. Genet.* **78**, 659 (2006).
14. Z. D. Zhang, A. Frankish, T. Hunt, J. Harrow, M. Gerstein, *Genome Biol.* **11**, R26 (2010).
15. B. Yngvadottir *et al.*, *Am. J. Hum. Genet.* **84**, 224 (2009).
16. J. R. Lupski *et al.*, *N. Engl. J. Med.* **362**, 1181 (2010).
17. J. M. Chen, D. N. Cooper, N. Chuzhanova, C. Férec, G. P. Patrinos, *Nat. Rev. Genet.* **8**, 762 (2007).
18. C. Casola, U. Zekonyte, A. D. Phillips, D. N. Cooper, M. W. Hahn, *Genome Res.* 10.1101/gr.127738.111 (2011).
19. N. Huang, I. Lee, E. M. Marcotte, M. E. Hurles, *PLoS Genet.* **6**, e1001154 (2010).
20. Y. Ishimaru *et al.*, *Proc. Natl. Acad. Sci. U.S.A.* **103**, 12569 (2006).
21. A. L. Huang *et al.*, *Nature* **442**, 934 (2006).
22. Wellcome Trust Case Control Consortium, *Nature* **447**, 661 (2007).
23. D. F. Conrad *et al.*, *Nature* **464**, 704 (2010).
24. S. B. Montgomery *et al.*, *Nature* **464**, 773 (2010).
25. J. K. Pickrell *et al.*, *Nature* **464**, 768 (2010).
26. E. Nagy, L. E. Maquat, *Trends Biochem. Sci.* **23**, 198 (1998).
27. M. V. Olson, *Am. J. Hum. Genet.* **64**, 18 (1999).
28. A. E. Fry *et al.*, *Hum. Mol. Genet.* **18**, 2683 (2009).
29. A. H. Bittles, J. V. Neel, *Nat. Genet.* **8**, 117 (1994).
30. A. R. McCune *et al.*, *Science* **296**, 2398 (2002).

Acknowledgments: T. Shah provided the Pyvoker software used for manual assignment of genotypes based on intensity clusters; S. Edkins was involved in the Sequenom validation; and the genotyping groups at Illumina, the Wellcome Trust Sanger Institute, and The Broad Institute of Harvard and MIT provided raw intensity data for the three Illumina arrays used for genotyping validation. The work performed at the Wellcome Trust Sanger Institute was supported by Wellcome Trust grant 098051; D.G.M. was supported by a fellowship from the Australian National Health and Medical Research Council; G.L. by the Wellcome Trust (090532/Z/09/Z); E.T.D. and S.B.M. by the Swiss National Science Foundation, the Louis Jeantet Foundation, and the NIH–National Institute of Mental Health GTEx fund; K.Y. by the Netherlands Organisation for Scientific Research (NWO) VENI grant 639.021.125; and H.Z., Y.L., and J.W. by a National Basic Research Program of China (973 program no. 2011CB809200), the National Natural Science Foundation of China (30725008, 30890032, 30811130531), the Chinese 863 program (2006AA02A302, 2009AA022707), the Shenzhen Municipal Government of China (grants JC200903190767A, JC200903190772A, ZYC200903240076A, CXB200903110066A, ZYC200903240077A, and ZYC200903240080A), and the Ole Rømer grant from the Danish Natural Science Research Council, as well as funding from the Shenzhen Municipal Government and the Local Government of Yantian District of Shenzhen. M.B.G. and C.T.-S. contributed equally to this work as senior authors. J.K.P. is on the scientific advisory board of 23andMe, and R.A.G. has a shared investment in Life Technologies. Raw sequence data for the 1000 Genomes pilot projects are available from www.1000genomes.org, and a curated list of the loss-of-function variants described in this manuscript is provided in the supporting online material.

Supporting Online Material

www.sciencemag.org/cgi/content/full/335/6070/823/DC1
Materials and Methods
Figs. S1 to S5
Tables S1 to S10
References (*31*–*71*)
Data Files S1 to S3

10 October 2011; accepted 11 January 2012
10.1126/science.1215040

REPORTS

Unraveling the Spin Polarization of the ν = 5/2 Fractional Quantum Hall State

L. Tiemann,[1,2]* G. Gamez,[1] N. Kumada,[1] K. Muraki[1,2]*

The fractional quantum Hall (FQH) effect at filling factor ν = 5/2 has recently come under close scrutiny, as its ground state may possess quasi-particle excitations obeying nonabelian statistics, a property sought for topologically protected quantum operations. However, its microscopic origin remains unknown, and candidate model wave functions include those with undesirable abelian statistics. We report direct measurements of the electron spin polarization of the ν = 5/2 FQH state using resistively detected nuclear magnetic resonance. We find the system to be fully polarized, which unambiguously rules out the most likely abelian contender and lends strong support for the ν = 5/2 state being nonabelian. Our measurements reveal an intrinsically different nature of interaction in the first excited Landau level underlying the physics at ν = 5/2.

When a highly correlated two-dimensional electron system (2DES) is placed under a strong perpendicular magnetic field B at low temperature, the interplay between quantum mechanics and the interelectron interaction produces spectacular effects. When the filling factor ν, the ratio between the number of electrons (n_s) and the number of magnetic flux quanta [$n_\phi = (e/h)B$; e: electron charge; h: Planck's constant], takes particular "magic" rational values p/q (p, q: integer), an energy gap forms based purely on electron correlation and makes the system's transverse (Hall) resistance invariant to small perturbations (*1*). In these fractional quantum Hall (FQH) phases, small variations of n_s or n_ϕ generate quasiparticles with a fractional charge $e^* = \pm e/q$ (*2*). The composite-fermion (CF) model (*3*), in which an electron is transformed into a fictitious particle by merging it with an even number of flux quanta, explains FQH effects for odd values of q. The most notable FQH state with an even denominator observed to date, the ν = 5/2 FQH state (*4*), cannot be described within this simple CF picture, and it has recently come under close scrutiny as it may support something even more tantalizing: a nonabelian state of matter (*5*–*7*). Charge excitations from this potential nonabelian state would be carried by quasiparticles whose interchange takes the system from one of its many ground states to another, whereas the interchange of ordinary abelian quasiparticles only adds a phase to their wave functions. This unusual property, specific to nonabelian states, is proposed as the foundation for topological quantum computation that would be robust against environmental decoherence (*8*). Both nonabelian (*5*, *9*, *10*) and abelian (*11*) states have been proposed for ν = 5/2, but experimental efforts (*12*–*16*) have not discriminated clearly between them. Two most probable wave function candidates that emerged through quasiparticle tunneling experiments on ν = 5/2 (*13*) are the nonabelian anti-Pfaffian state (*9*, *10*) and the abelian (331) state (*11*). One can discriminate between them by measuring the spin polarization of the state (*17*–*19*), as the former is fully polarized, and the latter unpolarized (*18*, *19*).

We perform this measurement using a 100-μm-wide Hall bar (Fig. 1A) with the 2DES confined to a 27-nm-wide gallium arsenide (GaAs) quantum well. A back gate enables us to tune the electron density n from 0.5×10^{15} to 4.2×10^{15} m^{-2}. At $n = 4.2 \times 10^{15}$ m^{-2}, the longitudinal resistance R_{xx} and the Hall resistance R_{xy} show a well-developed ν = 5/2 FQH state at 12 mK, along with pronounced FQH features at ν = 7/3 and 8/3, indicating a high sample quality (*20*) (Fig. 1B).

Our measurement of the spin polarization exploits the hyperfine interaction that intrinsically exists between the magnetic moments of the atoms constituting the GaAs quantum well and the spins of the electrons confined therein. When the 2DES has a nonzero spin polarization P, nuclei in contact with the 2DES experience a local magnetic field, which shifts their nuclear resonance frequency to a lower value by an amount proportional to P (Knight shift K_s). We measure K_s using the resistively detected nuclear magnetic resonance (RD-NMR) technique (*21*), where the resonant absorption of radio frequency (rf) and the resultant change in the nuclear polarization

[1]NTT Basic Research Laboratories, NTT Corporation, 3-1 Morinosato-Wakamiya, Atsugi 243-0198, Japan. [2]ERATO Nuclear Spin Electronics Project, Japan Science and Technology Agency (JST), Kawaguchi 332-0012, Japan.

*To whom correspondence should be addressed. E-mail: lars.tiemann@gmail.com (L.T.); muraki.koji@lab.ntt.co.jp (K.M.)

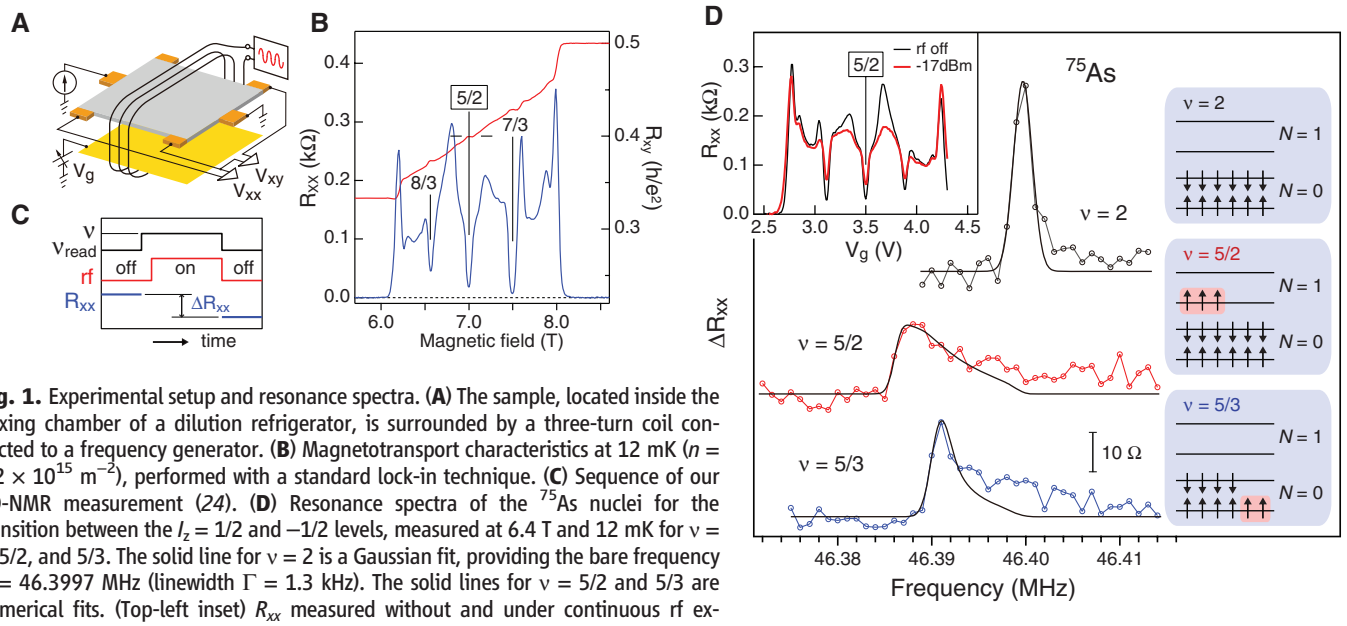

Fig. 1. Experimental setup and resonance spectra. (**A**) The sample, located inside the mixing chamber of a dilution refrigerator, is surrounded by a three-turn coil connected to a frequency generator. (**B**) Magnetotransport characteristics at 12 mK (n = 4.2 × 10^{15} m^{-2}), performed with a standard lock-in technique. (**C**) Sequence of our RD-NMR measurement (*24*). (**D**) Resonance spectra of the ^{75}As nuclei for the transition between the I_z = 1/2 and −1/2 levels, measured at 6.4 T and 12 mK for ν = 2, 5/2, and 5/3. The solid line for ν = 2 is a Gaussian fit, providing the bare frequency f_0 = 46.3997 MHz (linewidth Γ = 1.3 kHz). The solid lines for ν = 5/2 and 5/3 are numerical fits. (Top-left inset) R_{xx} measured without and under continuous rf excitation with −17 dBm, the output power we used to obtain spectra. (Right insets) LL energy diagrams and their occupations. The number of electron spins that can contribute to K_s (highlighted in red) is 1.5 times larger at ν = 5/2 than at ν = 5/3.

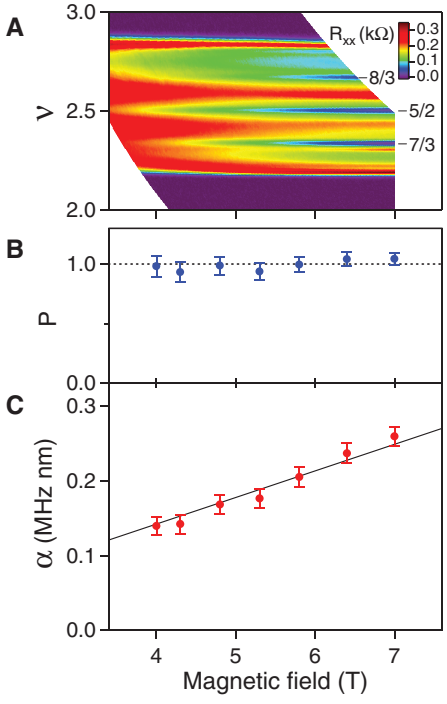

Fig. 2. Magnetic-field dependence of Knight shift and spin polarization at ν = 5/2. (**A**) Mapping of R_{xx} plotted as a function of B and ν. (**B**) Polarization calculated as $P = \alpha/\alpha_{full}(B)$. (**C**) Parameter α deduced from the fitting of resonance spectra measured at ν = 5/2 at different values of B. The solid line represents a function $\alpha_{full}(B) \propto B$ obtained from a linear fit. [For the estimation of error bars, see (*24*).]

$\langle I_z \rangle$ are detected as a change in R_{xx} that originates from the coupling between $\langle I_z \rangle$ and the electron Zeeman energy $E_Z \propto (B + b_0 \cdot \langle I_z \rangle)$ mediated by the hyperfine interaction (b_0: constant). To deduce P from the NMR spectrum measured at ν = 5/2, we also measure states with known spin polarizations at ν = 2 and 5/3 at the same B, from which the bare unshifted resonance frequency of the nuclei and the proportionality factor between P and K_s are deduced. Standard RD-NMR, however, is not directly applicable: At ν = 2 and 5/3, R_{xx} is zero, whereas at ν = 5/2, it only showed nonresonant heating effects. We therefore use the back gate to switch to a different filling factor ν_{read} with finite R_{xx} and sensitivity to read out the resonant rf absorption at ν as a change in R_{xx} at ν_{read} (Fig. 1C) (*22*). We used ν_{read} = 0.59 to 0.65, where R_{xx} becomes highly sensitive to tiny perturbations in E_Z due to the competition between differently spin-polarized FQH ground states (*23*, *24*). The ν = 5/2 FQH state remains well developed during our NMR measurements (Fig. 1D).

Figure 1D shows resonance spectra of the ^{75}As nuclei measured for three different filling factors at 6.4 T. The top spectrum was measured at ν = 2, where the 2DES is unpolarized because equal numbers of spin-up and spin-down electrons fill the two lowest Landau (LL) levels, (N = 0, ↑) and (N = 0, ↓) (right inset). The peak's center thus marks the unshifted resonance frequency of the ^{75}As nuclei. When RD-NMR is performed at ν = 5/2 (= 2 + 1/2), we find that the resulting resonance spectrum is Knight shifted to a lower frequency, indicating a nonzero polarization. We compare the ν = 5/2 spectrum with the spectrum at ν = 5/3 (= 2 − 1/3), a FQH state whose effective spin polarization is equal to that of the fully polarized ν = 1/3 Laughlin state (*2*). We accessed different values of ν by changing the number of electrons while keeping B constant. Thus, the Knight shift for ν = 5/2 should be 1.5 times larger than that for ν = 5/3, if both states are fully polarized (right insets).

For an accurate determination of the spin polarization, we take account of the spectral shape for each ν. The spectra for ν = 5/2 and 5/3 are asymmetrically broadened, reflecting the local electron density (determined by the probability density of the subband wave function $|\Psi_\nu(z)|^2$) that varies along the z direction. We fit these spectra by calculating the Knight shift $K_s(z) = \alpha_\nu \cdot |\Psi_\nu(z)|^2$ for each nucleus and then integrating over z, with α_ν the fitting parameter representing the size of the Knight shift (*24*). Taking the electron densities contributing to the polarization into account, we find that $\alpha_{5/2}/\alpha_{5/3}$ = 1.56 obtained from the fit corresponds to a polarization ratio of $P_{5/2}/P_{5/3}$ = 1.04. This clearly shows that the ν = 5/2 FQH state is fully polarized.

An open question is whether the ν = 5/2 FQH state remains fully polarized as the Zeeman energy is decreased. When we fit the ν = 5/2 spectra measured at different values of B, the obtained parameter α follows a linear function reflecting the density of electrons contributing to K_S that is proportional to B (Fig. 2C). This result indicates that the polarization is constant, independent of the Zeeman energy between 4.0 and 7.0 T (Fig. 2B). Mapping R_{xx} over the same range of B shows that the ν = 5/2 FQH minimum evolves continuously (Fig. 2A). The absence of a singularity is consistent with the system being polarized over the entire density range.

With these measurements, which provide direct evidence of full polarization at ν = 5/2, we are able to exclude all unpolarized or partially polarized states as the correct description of the ν = 5/2 state. Moreover, we can unambiguously rule out the abelian (331) state (*11*), which had remained one of the most likely candidates through quasiparticle tunneling experiments (*13*). Other abelian models had already been ruled

out (*13*). Therefore, the remaining most likely models contain only nonabelian states, the anti-Pfaffian state (*9*, *10*), its particle-hole conjugate the Pfaffian state (*5*), and the $U(1) \times SU_2(2)$ state (*25*), which are all spin polarized and therefore consistent with our results. Although recent optical experiments suggest an unpolarized system (*26*) or partially polarized domains developing at $\nu = 5/2$ (*27*), its true ground state, as we have shown, is fully spin polarized (supplementary online text).

To better understand the physics behind the $\nu = 5/2$ FQH state and its polarization, we have explored other states in the $N = 1$ and $N = 0$ LLs (Fig. 3A) and mapped out the entire range of experimentally accessible ν at 6.4 T (Fig. 3, B and C). In the $N = 0$ LL between $\nu = 2$ and 1/3, α exhibits a complicated oscillatory pattern reflecting the various CF ground states (*28*). The dashed line in Fig. 3C represents the value of α expected for full polarization at each value of ν, calculated on the basis of three data points near $\nu = 5/3$. In addition to $\nu = 5/3$, other fully polarized quantum Hall states such as $\nu = 1$, 2/5, and 1/3 show maxima approaching the line of full polarization (*24*), whereas unpolarized FQH states such as $\nu = 4/3$ exhibit minima approaching zero. By contrast, in the $N = 1$ LL, α increases linearly for $\nu \geq 2.2$ across $\nu = 7/3$, 5/2, and up to 8/3, indicating that the system is fully polarized over the range investigated here (Fig. 3B).

Because this measurement is performed at constant B, neither the Zeeman energy ($\propto B$) nor its ratio to the Coulomb energy ($\propto B^{1/2}$) can account for these qualitative differences between the $N = 0$ and $N = 1$ LLs. Thus, the contrasting behavior reflects the character of the interparticle interaction (*29*). Notable examples can be found at half fillings. CFs do not pair up at and near $\nu = 1/2$ or 3/2 due to the strong repulsion at short distances (*30*), and the system is well described as a compressible Fermi sea of CFs, which naturally accounts for its partial polarization (*28*). At $\nu = 5/2$, the weak repulsion at short distances is believed to be essential for the pairing of CFs and the formation of the $\nu = 5/2$ FQH state (*30*, *31*).

The properties of unpaired CFs at $\nu = 5/2$, the parent state of the $\nu = 5/2$ FQH state, can be examined through RD-NMR measurements at elevated temperatures (Fig. 4B). Although the $\nu = 5/2$ FQH state has vanished at 150 mK (Fig. 4A), its polarization is unaffected and remains nearly maximal up to 200 mK, before it starts to gradually drop (Fig. 4C), in contrast to the polarization at $\nu = 3/2$ being constant. The robustness of the high polarization to temperature is seen in the entire $N = 1$ LL (Fig. 4D). Fitting the data in Fig. 4C by using a simple noninteracting CF model (*32*) yields a CF effective mass m_{CF} of $(2.68 \pm 0.24)m_e$ and $(0.71 \pm 0.05)m_e$ for $\nu = 5/2$ and 3/2, respectively (m_e: electron mass in vacuum). In this simple picture, the high spin polarization is explained in terms of the large m_{CF} in the $N = 1$ LL, making the Fermi level smaller than E_Z. It is thus tempting to consider the large m_{CF} to be

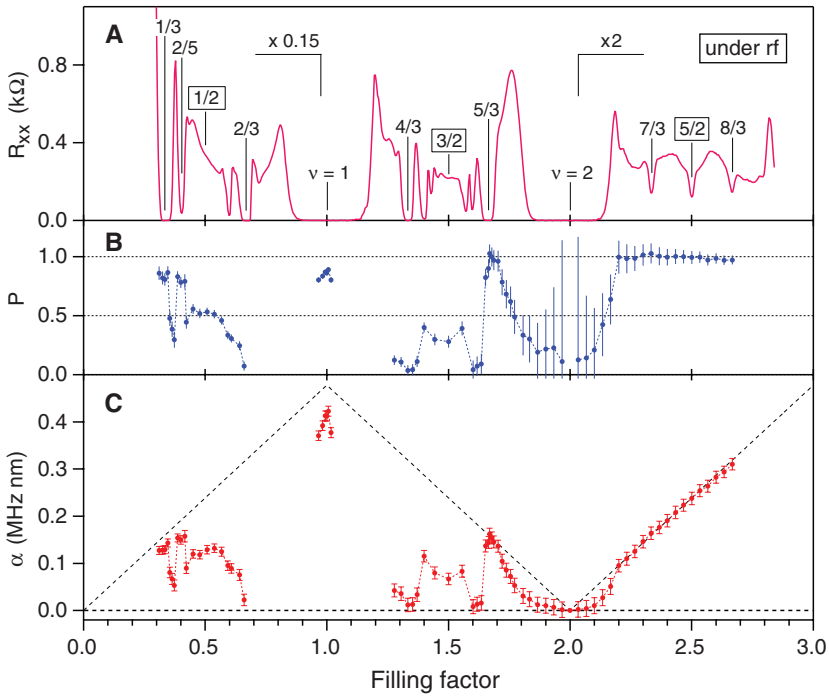

Fig. 3. RD-NMR at different filling factors. (**A**) R_{xx} measured under continuous application of rf with the same power (–17 dBm) as used for the RD-NMR measurement. (**B**) Polarization P calculated as $P = \alpha/\alpha_{full}(\nu)$. (**C**) Parameter α deduced from fitting the spectra (e.g., fig. S2) measured at 6.4 T and 12 mK. The dashed line represents the value $\alpha_{full}(\nu)$ expected for full polarization at each value of ν (*24*).

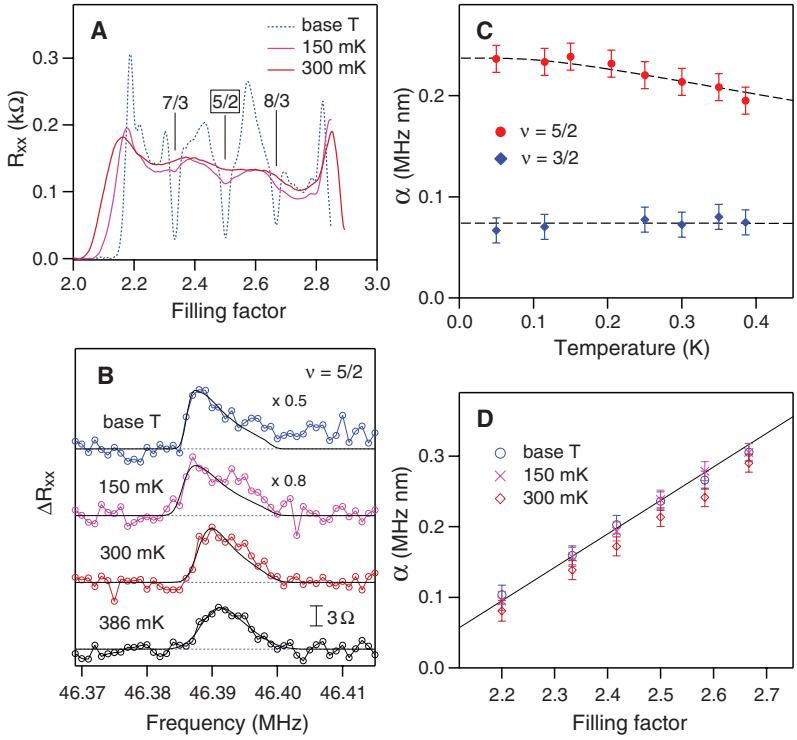

Fig. 4. Temperature dependence of Knight shift and polarization. (**A**) Magnetotransport characteristics at different temperatures and 6.4 T. (**B**) Resonance spectra measured at $\nu = 5/2$ at different temperatures. (**C**) Parameter α deduced from the fitting of resonance spectra measured at $\nu = 5/2$ and 3/2 at different temperatures. The dashed line represents a fitting based on a noninteracting CF model (*24*, *32*). (**D**) Parameter α for various values of ν in the $N = 1$ LL at different temperatures. The solid line represents the value expected for full polarization as determined from the data in Fig. 3C.

essential in the pairing of CFs and the formation of the ν = 5/2 FQH state at low temperature.

Our NMR experiments have demonstrated maximal spin polarization for the ν = 5/2 FQH state over a wide range of electron densities. These measurements are consistent with the nonabelian Pfaffian state (*5*) and the anti-Pfaffian state (*9*, *10*), while unambiguously ruling out the unpolarized (331) state (*11*), which had been the most likely abelian contender (*13*). However, the exciting prospect of topologically protected quantum operations using the ν = 5/2 FQH state awaits a direct experimental demonstration of its nonabelian nature.

References and Notes

1. D. C. Tsui, H. L. Stormer, A. C. Gossard, *Phys. Rev. Lett.* **48**, 1559 (1982).
2. R. B. Laughlin, *Phys. Rev. Lett.* **50**, 1395 (1983).
3. J. K. Jain, *Phys. Rev. Lett.* **63**, 199 (1989).
4. R. L. Willett *et al.*, *Phys. Rev. Lett.* **59**, 1776 (1987).
5. G. Moore, N. Read, *Nucl. Phys. B* **360**, 362 (1991).
6. M. Greiter, X. G. Wen, F. Wilczek, *Nucl. Phys. B* **374**, 567 (1992).
7. C. Nayak, F. Wilczek, *Nucl. Phys. B* **479**, 529 (1996).
8. C. Nayak, S. H. Simon, A. Stern, M. Freedman, S. Das Sarma, *Rev. Mod. Phys.* **80**, 1083 (2008).
9. M. Levin, B. I. Halperin, B. Rosenow, *Phys. Rev. Lett.* **99**, 236806 (2007).
10. S.-S. Lee, S. Ryu, C. Nayak, M. P. A. Fisher, *Phys. Rev. Lett.* **99**, 236807 (2007).
11. B. Halperin, *Helv. Phys. Acta* **56**, 75 (1983).
12. M. Dolev, M. Heiblum, V. Umansky, A. Stern, D. Mahalu, *Nature* **452**, 829 (2008).
13. I. P. Radu *et al.*, *Science* **320**, 899 (2008).
14. R. L. Willett, L. N. Pfeiffer, K. W. West, *Proc. Natl. Acad. Sci. U.S.A.* **106**, 8853 (2009).
15. V. Venkatachalam, A. Yacoby, L. Pfeiffer, K. West, *Nature* **469**, 185 (2011).
16. A. Bid *et al.*, *Nature* **466**, 585 (2010).
17. R. Morf, *Phys. Rev. Lett.* **80**, 1505 (1998).
18. I. Dimov, B. I. Halperin, C. Nayak, *Phys. Rev. Lett.* **100**, 126804 (2008).
19. A. E. Feiguin, E. Rezayi, K. Yang, C. Nayak, S. Das Sarma, *Phys. Rev. B* **79**, 115322 (2009).
20. G. Gamez, K. Muraki, ν=5/2 fractional quantum Hall state in low-mobility electron systems: Different roles of disorder; available at http://arxiv.org/abs/1101.5856 (2011).
21. W. Desrat *et al.*, *Phys. Rev. Lett.* **88**, 256807 (2002).
22. N. Kumada, K. Muraki, Y. Hirayama, *Phys. Rev. Lett.* **99**, 076805 (2007).
23. J. H. Smet *et al.*, *Nature* **415**, 281 (2002).
24. Materials and methods are available as supporting material on *Science* Online.
25. X. G. Wen, *Phys. Rev. Lett.* **66**, 802 (1991).
26. M. Stern *et al.*, *Phys. Rev. Lett.* **105**, 096801 (2010).
27. T. D. Rhone *et al.*, *Phys. Rev. Lett.* **106**, 196805 (2011).
28. I. V. Kukushkin, K. von Klitzing, K. Eberl, *Phys. Rev. Lett.* **82**, 3665 (1999).
29. F. D. M. Haldane, *Phys. Rev. Lett.* **51**, 605 (1983).
30. V. W. Scarola, K. Park, J. K. Jain, *Nature* **406**, 863 (2000).
31. N. Read, D. Green, *Phys. Rev. B* **61**, 10267 (2000).
32. N. Freytag, M. Horvatić, C. Berthier, M. Shayegan, L. P. Lévy, *Phys. Rev. Lett.* **89**, 246804 (2002).

Author contributions: L.T. performed all the RD-NMR and transport measurements presented in this paper. G.G. performed transport measurements to optimize the samples. N.K. advised on the RD-NMR measurements. K.M. grew heterostructures and fabricated samples. L.T. and K.M. analyzed the data and wrote the paper.

Supporting Online Material

www.sciencemag.org/cgi/content/full/science.1216697/DC1
Materials and Methods
Supplementary Text
Figs. S1 and S2
References (*33*–*45*)

2 August 2011; accepted 19 January 2012
Published online 26 January 2012;
10.1126/science.1216697

A Logic-Gated Nanorobot for Targeted Transport of Molecular Payloads

Shawn M. Douglas,* Ido Bachelet,* George M. Church†

We describe an autonomous DNA nanorobot capable of transporting molecular payloads to cells, sensing cell surface inputs for conditional, triggered activation, and reconfiguring its structure for payload delivery. The device can be loaded with a variety of materials in a highly organized fashion and is controlled by an aptamer-encoded logic gate, enabling it to respond to a wide array of cues. We implemented several different logical AND gates and demonstrate their efficacy in selective regulation of nanorobot function. As a proof of principle, nanorobots loaded with combinations of antibody fragments were used in two different types of cell-signaling stimulation in tissue culture. Our prototype could inspire new designs with different selectivities and biologically active payloads for cell-targeting tasks.

The DNA origami method (*1*), in which a multiple-kilobase single-stranded "scaffold" is folded into a custom shape by interaction with hundreds of oligonucleotide "staple" strands, has proved to be extremely versatile for creating custom two- and three-dimensional assemblies (*2*–*4*) that can template precise arrangement of diverse components (*5*–*7*). DNA can also be used to construct devices that perform robotic tasks such as sensing, computation, and actuation (*8*–*11*). Recently, a three-dimensional DNA origami box integrating both structural and computational components was described (*12*). Inspired by these advances, we sought to design a robotic DNA device capable of selectively interfacing with cells to deliver signaling molecules to cell surfaces.

Using cadnano, a computer-aided design tool for DNA origami (*13*), we created a nanorobot in the form of a hexagonal barrel with dimensions of 35 nm × 35 nm × 45 nm. The barrel consists of two domains that are covalently attached in the rear by single-stranded scaffold hinges, and can be noncovalently fastened in the front by staples modified with DNA aptamer–based locks (Fig. 1A). Initial self-assembly proceeds in a one-pot reaction in which 196 oligonucleotide staple strands direct a 7308-base filamentous phage–derived scaffold strand into its target shape during a thermal-annealing ramp of rapid heating followed by slow cooling (*14*).

A clasp system based on DNA locks and DNA keys was previously used to control the opening of the lid on a DNA box (*12*). To operate our device in response to proteins, we designed a DNA aptamer–based lock mechanism that opens in response to binding antigen keys (Fig. 1, B and C). Our lock system was inspired by aptamer beacons (*15*) and structure-switching aptamers (*16*), which typically undergo target-induced switching between an aptamer-complement duplex and an aptamer-target complex. We incorporated aptamer-complement duplexes on the left and right sides of the front of the barrel, such that the aptamer strands are attached to one domain and partially complementary strands are attached to the other domain. When both aptamers recognize their targets, the lock duplexes dissociate, and the nanorobot—acting as an entropic spring—undergoes a drastic reconfiguration to expose its previously sequestered surfaces. We found that shorter duplexes gave better sensitivity and faster activation rates, but at a cost of increased spontaneous activation (see text S2). We chose a lock duplex length of 23 base pairs (bp) for subsequent experiments because it displayed similar sensitivity to a shorter 16-bp duplex (activation at 10 pM) without the unacceptable loss in sensitivity observed for longer duplexes (30, 37, and 44 bp required 1 nM).

Payloads that were premodified by covalent attachment to the 5′ end of a 15-base single-stranded DNA oligonucleotide linker were loaded inside the nanorobot. To enable multivalent interaction with surface receptors for potent cell stimulation (*17*), we aimed to load at least two payload molecules per robot. Twelve payload attachment sites were arranged in an inward-facing ring in the middle of the barrel (Fig. 1, A and C) to enable different payload orientations and spacings. The sites are staple strands with 3′ extensions

Wyss Institute for Biologically Inspired Engineering and Department of Genetics, Harvard Medical School, Boston, MA 02115, USA.

*These authors contributed equally to this work.
†To whom correspondence should be addressed. E-mail: http://arep.med.harvard.edu/gmc/email.html